Moxifloxacin Inhibited β-Amyloid Bio-communication and Impairs Aβ Refolding with HSP60 and HSP60/MMP-2 Devices for Promoting Cell Normal Reversible Membrane Potential

E. T. Chen[*], J. T. Thornton[**], S-H. Duh[***]

[*]Advanced Biomimetic Sensors, Inc., 6710A Rockledge Drive,
Bethesda, MD 20817, USA, ellen@abs-isensors.com
[**] Bruker Nano, 19 Fortune Dr., Billerica, MA 01821, USA
[***]University of Maryland Medical System, 22 South Greene St, Baltimore, MD 21201, USA

ABSTRACT

Moonlighting proteins, such as Heat Shock Protein (HSP) and Matrix Metalloproteinase (MMP) protein, played roles in human diseases. We developed an HSP60 memristive device and an HSP/MMP-2 superconductive device for assessing a protein, Aβ refolding intrinsic energy landscape change by monitoring the antibiotic drug moxifloxacin (MOX)'s real-time effect on such change at different dosages. Sensor 1 was developed by cross-linking HSP60 with conductive polymers on gold chips. Sensor 2 was fabricated by self-assembling the HSP60 polymer mixtures on the top of an innate MMP-2/copolymer membrane. Results showed MOX impaired Aβ's refolding in the HSP's cavity in real-time monitoring of the open circuit potential (OPO) change against controls. We used a Double-step chronopotentiometry (DSCPO) method to evaluate MOX's effectiveness in promoting reversible membrane potential (RMP) values in the safe zoon for the two sensors. Sensor 2 demonstrated the ability to expel Aβ and promote normal RPM with an accuracy 97.3% and imprecision 0.05%, which was not dependent on MOX concentrations. Sensor 1 showed a lower accuracy rate, and it was dependent on MOX concentration.

***Keywords*:** memristive sensor, MMP2/HSP60 network, reversible membrane potential, antibiotics; inhibition of Aβ refolding; Dosage kinetics

1. INTRODUCTION

Protein moonlighting is a phenomenon that proteins perform two or more unrelated functions that are directly impacting human health [1-5]. MMPs and HSPs were well-known moonlighting proteins. Originally MMPs is known for their localization at the extracellular matrix (ECM), and have the role of degrading ECM proteins [1-5], but accumulated literature reported MMPs have been found in every cell compartment, such as in cytoplasm, in cell nuclei, and in mitochondria playing roles in apoptosis, tumor invasion, genetic instability, and innate immunity functionalities [1-7]. HSPs/MMPs working as a team to influence our immune system have been reported based on their moonlighting capabilities and unique behaviors [1-7]. This moonlighting catastrophic event may cause vulnerable to cancer patients, diabetes, coronary artery disease patients, and Alzheimer's patients when an unusual viral attacked, like SARS-CoV 2 viral in the pandemic, that a report had shown 50% upregulated genes among the top 10 infected human genes are belong to HSP family in the Covid 19 cases [8]. β-Amyloid and hyperglycemia can activate MMP-2 in the mitochondrial cell causing MMP-2 concentration increase, and it decreases the Heat Shock Protein (HSP) 60's concentration, which leads to disturbing the mitochondrial gap membrane potential, causes mitochondria cell dysfunction and released cytochrome c to apoptosis immune cells, hence, protein MMP/HSP network moonlighting contributes to many diseases [1-10].

Fluoroquinolones, levofloxacin, and moxifloxacin (MOX) prove to be clinically beneficial as adjunct treatment therapeutic agents for the management of severe Covid 19 patients worldwide according to reports in the literature [11-14]. There is very few, if any, to study the links between the Moon-lighting protein network of HSP/MMP with the proven effective antibiotics, such as moxifloxacin interacting with Aβ because of the high percentage of the mortality rate of Covid 19 is elderly who had significant underline diseases of Alzheimer's and dementia. The initial goal of this research project is to develop an HSP60/MMP-2 model device for evaluation of the MOX effectiveness to impair HSP60's function and lead to recover the reversible membrane potential in the presence of impact from Aβ compared with an HSP control device. Our prior research reported an innate HSP60/MMP-2 network protein device with cross-linked polymers forming superconductive and memristive nanostructured toroidal-tower array self-assembled membrane (SAM), was able to direct ultra-sensitively sensing multiple biomarkers, such as glucose, pyruvate, acetyl CoA, and choline, under antibody-free, label-free and tracer-free conditions [15]. The evidence implied that the HSP/MMP device mimicked the moon-lighting protein HSP/MMP network's characteristics. Under this discovery, we attempted to put this system under testing of its biocommunication with moxifloxacin with or without the impact of Aβ. Following Sections, we explain the methods used for evaluation of the protein refolding landscape energy changes with or without

MOX in the presence of Aβ under antibody-free, labeling-free, reagent-free, and tracer-free conditions.

2. RESULTS AND DISCUSSIONS

2.1 The Friedel-oscillation in the Superlattice Membranes

Friedel-oscillation is a phenomenon of long-range indirect interactions between electrons on a superlattice surface by metal oxide materials [16]. Our group has observed strong Friedel- oscillation events in AFM images based on mono- or multiple-layered organo-metallic materials on SAM surfaces [17-22]. Fig. 1A depicts a 3D AFM image of Sensor 1. Fig. 1B has many vertically oriented nano-pillars on top of horizontally oriented well-ordered high and low-lay densified nanotubes. Fig. 1C reveals a cluster of 37 two-heptametrical rings made up tetradecamer oriented chaperone HSP60, and a 37 cluster of U-shape HSP60 subunit was observed on top of the layered nanotube surface. The ratio of width/length of the HSP cluster of 0.90 vs 0.88 reported from the literature, has a good agreement vs. cryo-EM of 98% [23-25]. Fig. 1D reveals the HSP60 cluster's structure.

Fig. 2A depicts the toroidal AFM image of an innate state MMP-2 comprised of a zinc finger connected with cysteine, and we observed the Friedel-oscillation in the 3D AFM image with an electronic cloud surrounded on the zinc atoms of the toroidal array superlattice. Fig. 2B shows the AFM image having large circulars with zinc created a Josephson junction superconducting qubit device. Fig. 2C depicts an AFM image of the multiple-enzyme network membrane with multiple-cluster high tower structure as "Tesla Tower" having the tower diameters between 500 nm to 2.4 μm, and the towers' height is about 500 nm. The strong Friedel- oscillation from Cooper-pair electron cloud due to the MMP-2...HSP60 networking alignment was observed. We observed many MMP-2 formed toroidal rings with some of them have zinc atoms on top. Fig. 2D depicts such a perfect "wedding ring" with zinc ions mobile from the bottom layer (z value 25.5 nm) to the second layer (z value 86.4 nm) sparkling. Many HSP60's fingerprint structure looks like two-end cut pineapple observed along with subunits on the superlattice flat surface.

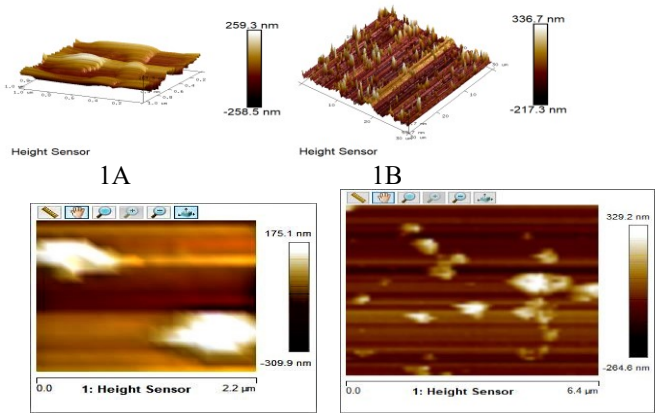

1A 1B

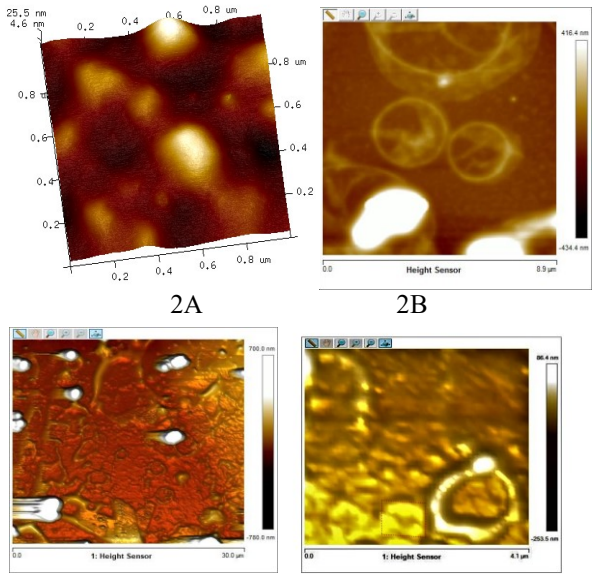

1C 1D

2A 2B

2C 2D

Fig. 1A depicts Sensor 1 of the HSP60 SAM's 3D image in an area of 1.0 x1.0 μm^2 with a ±Z-value 259.3 nm. Fig. 1B depicts the 3D AFM image. Fig. 1C depicts the HSP60 cluster on the right -side corner, and the subunit cluster on the top left-side corner. Fig. 1D depicts the top view of the HSP60 nanopore rings and the side view of the HSP60 structure. Fig. 2A depicts the 3D AFM image of the MMP-2 toroidal array superlattice membrane as the first layer in Sensor 2. Fig. 2B depicts the 2D AFM image in a larger area. Fig. 2C depicts the second layer of tower structure HSP60 AFM image multiple-enzyme network membrane which is on top of the first layer of MMP-2. Fig. 2D depicts the toroidal "diamond ring" structure in detail.

2.2 Moxifloxacin's Influence on the i-V Curves in the Presence of Aβ using a CV Method

2.2.1 Memristivity and Superconductivity

Memristors are devices made of nanolayers that can mimic neuronal synapses with a characteristic of a hysteresis loop in the i-V curve [26-32]. The memristor HSP Sensor 1's hysteretic i-V profiles measured by the CV method are presented in Fig. 3 as control shown in scan rate 20 Hz, 200 Hz, and 1 kHz with the cross-point at zero-bias having zero current, except, 10 kHz and 20 kHz lost the memristivity. At 20 Hz, the i-V curve shown Aβ alone having two significant oxidative DET_{ox} peaks at 189 mV and 465 mV, but after MOX applied in the Aβ solution, no DET_{ox} peaks were observed, indicating MOX had impaired HSP60's function. In contrast, the HSP60/MMP-2 Sensor 2 shows no DET_{ox} peaks of Aβ in all scan rates. Fig. 4 Panel A at 20 Hz, a large reduction DET_{red} peak at –438 mV was observed, indicates Sensor 2 transferred Aβ state from harmful to the useful. At 20 kHz, the superconductivity at zero-bias was observed for with or without Aβ, and for with or without MOX in Fig. 4 Panel B. The phase change and superpositioning were also observed [17, 19-22, 33-35]. These observations indicate

Sensor 2 expelled Aβ enter HSP's cavity based on its unique toroidal/tower structure.

Zinc ions' mobility from MMP-2's superlattice toroidal array layer efflux toward HSP 60's double-ring structured layer and formed a long-range DET relay shown in Fig. 2B and 2D. This research confirms clinical doctors' suggestions for adding zinc ionophores for Covid 19 patients' treatments, which based on our structural and neuronal circuitry's perspectives [40-42].

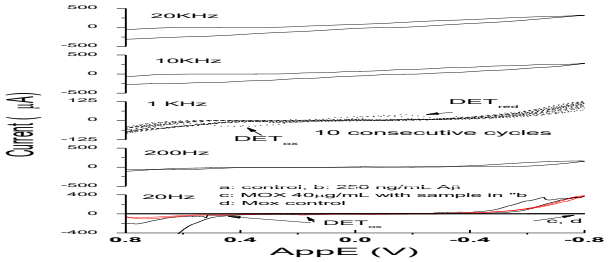

Fig. 3 depicts Sensor 1's i-V curves of controls over different scan rates. At 20Hz, compared curves of MOX affecting Aβ.

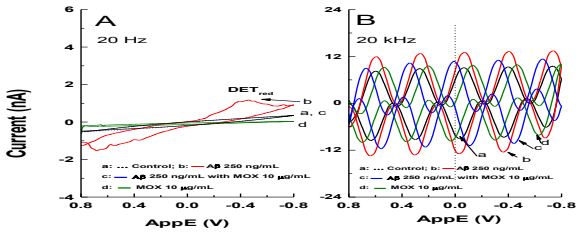

Fig. 4 depicts Sensor 2 MOX affecting I-V curves of Aβ at 20Hz (Panel A) and 20 kHz (Panel B) compared with controls.

2.3 Pharmacodynamic Model Devices to Study Aβ Protein-folding Inhibitions Using an OPO Method

2.3.1. The Open Circuit Potential (OPO) of Sensor 1

Scientists revealed proteins have a funnel-shaped energy landscape with many high-energy, unfolded structures and only a few low-energy, folded structures [40-42]. We expected our devices can be models for assessing protein-folding energy under an open circuit potential (OPO) condition. Here, the results from the potential vs. time curves shown in Fig. 5 for Sensor 1 are of 2-, 6-, and 12-minutes monitoring of the Aβ folding energy landscape with 250 ng/mL Aβ compared with buffer controls. Curves with Aβ alone, energy dropped to negative from original equilibrium state was observed, and the data was compared through fitting a polynomial third-order model of $y=A + \beta1*X + \beta2*X^{\wedge 2} + \beta3* X^{\wedge 3}$, β1 refers to the coefficient of the linear component, β2, and β3 refer to the coefficient of the curvature, the values of β1 is 0.00184 at 2 minutes monitoring, which is the highest and the β2 has the most negative down dropping power of $-5.89e^{-5}$ than at 4 and 12 minutes monitoring, indicates HSP60 alone is vulnerable to toxins' attack. The three buffer control curves have the same first-order rate constant value of 0.98/s based on the exponential curve fitting Box Lucas 1MOD model $y= a(1-e^{-bx})$, as a result, showed a "healthy" HSP60 sensor in the buffer before Aβ attack. Fig. 6 in Panel A, compared the energy landscape curves at a fixed Aβ concentration with various MOX concentrations monitored at 2 minutes to 6 minutes shown in Panel B, demonstrates MOX's ability to impair Aβ folding completely with rate constants 0.9875/s ± 0.0047 (4 rate constant values) having an error of 0.76% related to the buffer control rate 0.98/s at 2 minutes monitoring; and a mean rate constant of 0.9877/s ± 0.0061 (5 rate constant values) with an error of 0.79% related to the buffer control rate 0.98/s at 6 minutes monitoring.

2.3.2. The Open Circuit Potential of Sensor 2

Device 2 of HSP60/MMP2 shown in Fig. 4A has the high Aβ concentration that did not cause any oxidative peaks, we further show under different MOX dosages, the potential vs. 2 minutes monitoring curves with the Aβ, no energy dropped to negative, compared with the buffer control was observed in Fig. 7. The mean rate constant value $0.987s^{-1}$ ± 0.0045 (n=4), produced an imprecision error of 0.16%, and a good agreement with the control's rate constant was obtained in 99.8%, except MOX at 0.5 μg/mL and 80 μg/mL, because curves drifting occurred and were failed to fit the model.

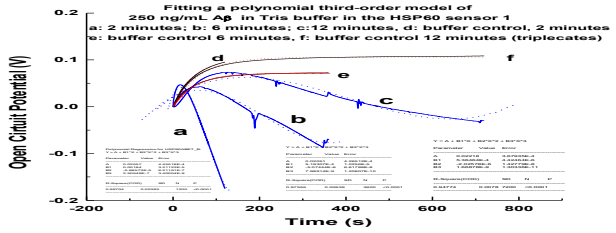

Fig. 5 depicts Sensor 1's 250 ng/mL Aβ effects on the open circuit potential vs. 2, 6, and 12 minutes monitoring of the energy change compared with controls.

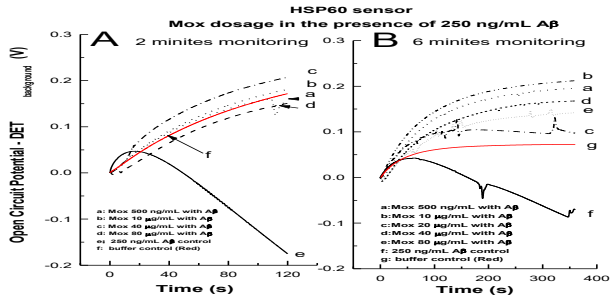

Fig. 6 depicts various concentrations of HOX impaired 250 ng/mL Aβ folding on the open circuit potential vs. 2 and 6 minutes compared with controls, respectively.

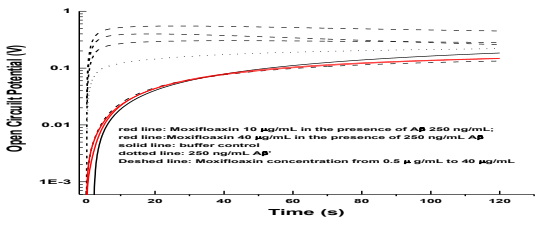

Fig. 7 depicts Sensor 2 (HSP60/MMP2) 's open circuit potential curves vs 2 minutes for monitoring the energy change over 500 ng/mL to 80 μg/mL MOX in the presence of 250 ng/mL Aβ compared with controls.

2.4 Recovery of the Reversible Membrane Potential (RMP) Through Moxifloxacin

Our group first reported using a ratio of action/resting potential to monitor the treatment of cancer in a 3D heat release map [27-30], because keeping a normal RMP is essential for maintaining healthy cells. Moxifloxacin changed the energy profiles of Sensor 1 as shown in Fig. 8 (L), that the voltage vs. time curves changed from asymmetric to symmetric when MOX concentration increases from 10 mg/mL to 80 mg/mL in the presence of 250 ng/mL Aβ vs. the controls. Fig. 8 (R) depicts Sensor 2's profiles, no asymmetric curves are observed under the same experimental conditions. The ratio of results is presented in Fig. 9 compared with the healthy ratio standard (0.8-1.5 at 95% CI). The MOX concentrations are safe in the range up to 20 µg/mL(n=9) in maintaining RMP, and 80 µg/mL is too far from the safe zoon when Aβ 250 ng/mL for Sensor 1. The 40 µg/mL MOX is out of safe zoon by 35.0% ± 0.2%. In contrast, Sensor 2's ratio values are all located in the safe zoon up to 80 µg/mL MOX (n= 18) compared with controls, indicates the HSP60/MMP2 moonlighting network enhanced the health states of cells' RPM by MOX inhibiting HSP's chaperoning function at a clinically harmful level Aβ.

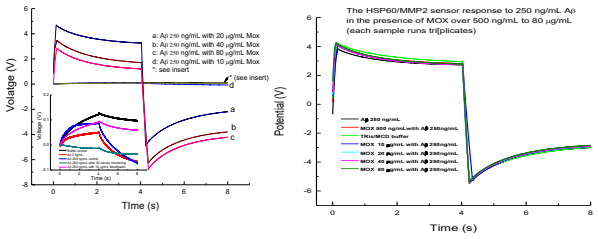

Fig. 8 (L) depicts the potential vs. time curves at ± 10 nA at MOX concentration from 10 to 80 µg/mLwith or w/o Aβ at 250 ng/mL for Sensor 1 (sample run triplicates). Fig. 8 (R) depicts Sensor 2's profiles with MOX from 0.5 to 80 µg/mL (5 levels) .

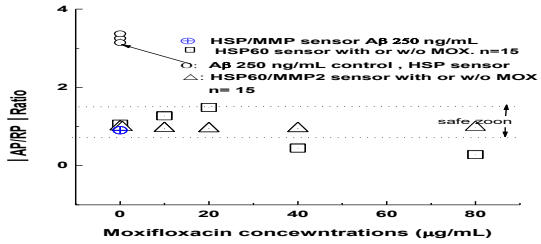

Fig. 9 depicts the comparison between Sensor 1 and Sensor 2 for the plots of AP/RP ratio vs. MOX concentration in the presence of 250 ng/mL Aβ over MOX from 0 to 80 µg/mL.

Table 1. Comparing performances of two sensors by linear regression method of |Ap/Rp| vs. MOX concentration with 250 ng/mL Aβ

Sensor	|Ap/Rp| Buffer only Mean (sd)	|Ap/Rp| 250 ng/mLAβ Mean (sd)	Interce pt	Slope	$S_{y/x}$	r	n	Accuracy Related to buffer control	Pooled sd (%) From 0 to 80 µg/mL	p
1[a]	1.06(0.006)	3.26(0.111)	1.06	0.02	0.004	0.9998	9	87.9%[b]	0.3%	< 0.0001
2[c]	0.995(4.5e-4)	0.90(0.004)	0.97	-9.4e-4	0.019	-0.01	18	97.3%	0.05%	< 0.955

[a]: HSP sensor has a L-S regression between 0 to 20 µg/mL MOX in the presence of 250 ng/mL Aβ. [b]: accuracy refers to the mean |Ap/Rp| value over that value of MOX between 0 to 80 µg/mL concentration divided by the mean of control. [c]: HSP60/MMP2 sensor has a regression over 0- 80 µg/mL in the presence of 250 ng/mL Aβ.

From results of L-S regression in Table 1, we conclude MOX shows RMP recovered for both sensors, only Sensor 1 shows a dependency of the Ap/Rp ratio values on the MOX concentration up to 20 µg/mL located in the safety zoon (n=9, $p<0.0001$), including the data in 40 and 80 µg/mL, an accuracy of 87.9% (n=15) produced related to the ratio of buffer, and a related pooled standard division of 0.3% was reached. Sensor 2 produced 97.3% accuracy result with a MOX range up to 80 µg/mL (n=18), further shows the ratio values are independent on MOX concentrations with an R-value of –0.01 and a slope $–9.4e^{-4}$ and $p<0.955$, that demonstrated a normal RPM is accomplishable over a wide MOX concentrations in the middle of an Aβ attacking.

3. EXPERIMENTAL

Sensor 1's membrane was fabricated by deposition of a solution comprised of HSP60, triacetyl-ß-cyclodextrin (TCD), polyethylene glycol diglycidyl ether (PEG), and poly (4-vinyl pyridine) (PVP) with appropriate propositions on the surface of gold chips at 37^0C for 72 hours. The procedures used for fabrication of the innate HSP60/MMP-2 Sensor 2 membrane were followed by published literature [15].

The morphology of the AU/SAM was characterized using an Atomic Force Microscope (AFM) (model Dimension Edge AFM, Bruker, MA). Data collected in TappingMode using silicon probes with a 5-10 nm tip radius and ~300kHz resonance frequency (Probe mode TESPA-V2, Bruker, MA).

All electrochemical data were collected by the Epsilon voltammetry working station with the software package for various methods applications (BASi, IN), and the figure plots, and statistical analysis, curve fitting was conducted using the OriginPro software package (OriginLab, MA).

4. CONCLUSIONS AND DISCUSSIONS

Assessing a protein, Aβ refolding intrinsic energy landscape change by monitoring the antibiotic drug MOX's real-time effect on such change at different dosages demonstrated the OPO method is viable. The results obtained correlated well with the results for evaluation of the RPM effect. Sensor 2 demonstrated the ability to maintain safe RPM values with high accuracy and was not dependent on MOX concentrations. The outcomes further highlight the moonlighting innate HSP60/MMP-2 network proteins' potential applications in providing patients with the possibility to effectively block Aβ refolding. The technology may find therapeutic applications in the future.

ACKNOWLEDGMENT

E. Chen thanks Dr. Kasica's help and discussions and also thanks to the NIST NanoLab for the clean room and other equipment used for this project.

REFERENCES

See www.abs-isensors.com